Available online at www.sciencedirect.com
SCIENCE DIRECT®
Microelectronic Engineering 75 (2004) 117–126
MICROELECTRONIC ENGINEERING
www.elsevier.com/locate/mee

X-ray microdiffraction: local stress distributions in polycrystalline and epitaxial thin films

M.A. Phillips [a], R. Spolenak [a,*], N. Tamura [b], W.L. Brown [c], A.A. MacDowell [b], R.S. Celestre [b], H.A. Padmore [b], B.W. Batterman [b,d], E. Arzt [a], J.R. Patel [b,e]

[a] *Max-Planck-Institut für Metallforschung, Heisenbergstrasse 3, D-70569 Stuttgart, Germany*
[b] *Advanced Light Source, LBNL, 1 Cyclotron Road, Berkeley, CA 94720, USA*
[c] *Department of Materials Science and Engineering, Lehigh University, Bethlehem, PA 18015, USA*
[d] *SSRL/SLAC, Stanford University, P.O. Box 43459, Stanford, CA 94309, USA*
[e] *Department of Materials Science and Engineering, Stanford University, Stanford, CA 94305, USA*

Received 4 October 2003; received in revised form 21 October 2003; accepted 12 December 2003
Available online 26 February 2004

Abstract

When investigated by X-ray microdiffraction, the stress states in thin metal films are found to be more complex than as assumed by the simple models that have been formulated to describe their behavior. In this paper, the local differences in stress have been measured in a polycrystalline Al(0.5 wt% Cu) film on Si and an epitaxial Cu film on Al_2O_3. Significant differences in stress state are apparent between grains, but also within grains. While both types of film display a local variation in residual stress state, the width of the distribution is much broader in the polycrystalline film. The reasons for this are discussed in terms of grain size distribution and dislocation nucleation.

Keywords: Microdiffraction; Thin films; Al; Cu; Al–Cu; Plasticity; Size effects; Synchrotron; Stress measurement

1. Introduction

Thin metal films on substrates are important for many technological applications, including microelectronic and micromechanical systems. It is now well known that materials in thin film form are stronger than the same materials in bulk form, such that the flow stresses increase with decreasing geometry (e.g. thickness) and microstructural dimensions. While much understanding has already been provided by careful experiments on thin films, principally using laser wafer curvature experiments, e.g. [1,2], the key to further understanding of deformation and strengthening in thin films is local measurement of stress and strain, i.e. by transmission electron microscopy (TEM) and X-ray microdiffraction (XRMD). In this paper, the

* Corresponding author. Tel.: +49-711-689-3416; fax: +49-711-689-3412.
E-mail address: spolenak@mf.mpg.de (R. Spolenak).

0167-9317/$ - see front matter © 2004 Elsevier B.V. All rights reserved.
doi:10.1016/j.mee.2003.12.053

local distribution of stresses in epitaxial and polycrystalline metal films is examined with the XRMD technique.

In general, it has been shown that film strength or film flow stress scales inversely with the film thickness. This can result in significant stresses in thin film devices, which in turn can lead to failure in service. Past work [3–5] has produced several models that provide a good description of the mechanisms that are involved in deformation of thin films. These models consider the energetics of strain relieved as a threading dislocation moves through a film versus the work required to lay down dislocations at interfaces between the film and substrate. The resulting expression, often referred to as the Nix–Freund model, usually takes a form like

$$\sigma_y = \frac{\sin\phi}{\cos\phi\cos\lambda}\frac{b}{4\pi(1-\nu)h}\left[\frac{2\mu_f\mu_s}{\mu_f+\mu_s}\ln\left(\frac{\beta h}{b}\right)\right], \tag{1}$$

where σ_y is the flow stress, h is the film thickness, μ_f and μ_s are the film and substrate shear moduli, ν is Poisson's ratio of the film material, b is the Burgers vector, β is a dislocation core-cut-off correction, and $\sin\phi/(\cos\phi\cos\lambda)$ is a geometric factor to account for texture and orientation of slip planes with respect to the film normal.

In recent work, Dehm et al. [6] have shown that epitaxial Al and Cu films can be adequately described by the Nix–Freund model. These are films with a large grain (or domain) size and sharply defined crystallographic interfaces between the metal film and substrate. Observation of dislocation motion within these epitaxial films also confirms the formation of threading dislocations. In polycrystalline films, an inverse-thickness relationship is also observed, however the flow stresses at room temperature are much higher than predicted by the Nix–Freund model. This is not unreasonable because the Nix–Freund model is not meant to include other strengthening mechanisms, such as effects of grain size [3]. Other authors (e.g. [4,7]) have included grain size terms to describe the general strength of thin films. However, in cases where the grain size is comparable to or even larger than the film thickness, as in the films examined here, the film thickness will dominate the yielding behavior.

TEM experiments [8,9] have shown that in polycrystalline and epitaxial films the amount of yielding (or plasticity) varies significantly with location. However, some of the inherent limitations of TEM (e.g. sample preparation, small field of view) make it difficult to directly correlate the TEM observations with macroscopic thin film behavior. TEM observations also do not give information on local strains, although some recent work with convergent beam electron diffraction (CBED) has been able to show asymmetries in the strain distribution [10] in thin film structures. Recent development of scanning microbeam X-ray diffraction has provided new insight into local plasticity in thin films. In this work, XRMD is used to examine polycrystalline Al(0.5 wt% Cu) on Si and epitaxial Cu on Al_2O_3. Previously, a large distribution of stresses was reported for the polycrystalline Al(Cu) film [11]. Here we provide a much larger data set for analysis and discussion. It will be shown that there are substantial differences between polycrystalline and epitaxial thin films in terms of stress distribution.

2. Sample preparation

The 1.5 μm thick Al(0.5 wt% Cu) thin film was magnetron sputter deposited at 400 °C on a 200 nm thick Si-rich (compared to stoichiometric Si_3N_4) SiN_x film on a Si wafer. The stress state at room temperature is primarily a result of the cooldown from the deposition temperature due to the difference in thermal expansion coefficients between the film and the substrate. In addition, some stress relaxation (creep) at room temperature has occurred over several weeks between cooldown and these measurements.

The 1 μm thick epitaxial Cu film was grown by magnetron sputtering on a (0 0 0 1)-oriented α-Al_2O_3 (sapphire) single crystal substrate. Deposition was performed at 100 °C, followed by a 10 min anneal at 600 °C. This film is one of the series characterized by Dehm et al. [6], and exhibits an orientation relationship that can be described by $\{1\,1\,1\} \pm \langle 1\,1\,2\rangle \mathrm{Cu} || (0\,0\,0\,1)\langle 1\,0\,\bar{1}\,0\rangle \mathrm{Al_2O_3}$. The data shown here are from the room temperature scans after one or two thermal cycles to 400 °C (“scan

1'', ''scan 2''). In typical thermal cycles, the behavior does not change after the first cycle, so the room temperature scans performed here are comparable. Data from the full temperature cycles for epitaxial copper on sapphire will be presented in a forthcoming paper.

3. X-ray microdiffraction

This study was conducted at the X-ray microdiffraction beam line (7.3.3) at the Advanced Light Source in Berkeley. In essence, white X-rays (6–14 keV) are focused to form a spot approximately 0.8×0.8 μm in size. Rather than moving the spot over the sample, a fixed diffracting geometry is used ($\omega = 45°$, $2\theta = 90°$) and a large area CCD camera is used to capture the diffraction information – in this case a Laue diffraction pattern from the illuminated volume. The Laue pattern is automatically indexed using software developed in-house to determine the orientation, stress and strain from the illuminated volume. Each CCD frame may contain multiple Laue patterns from different metal grains and the silicon substrate, and the software can also index these overlapping Laue patterns. The misorientation between any two grains as well as orientation variations within single grains can be determined with a precision of 0.01°. The deviations of the Laue spot positions from those of an unstrained crystal are used to calculate the distortion of the crystal unit cell, with a strain sensitivity of about 2×10^{-4}. The deviatoric stress tensor is then calculated using the anisotropic stiffness coefficients for the material. A more detailed description of the apparatus and technique is given elsewhere [12,13].

This paper reports the maximum resolved shear stress (MRSS) in each grain. The MRSS is calculated from the deviatoric stress tensor by determining the resolved shear stress on each of the twelve $\langle 1\,1\,0\rangle\{1\,1\,1\}$ slip systems and then taking the maximum absolute value. The error in the strain tensor results in a maximum error in the MRSS of 17 MPa for Al and 32 MPa for Cu.

Maintaining the fixed diffracting geometry, the sample is raster scanned with a piezoelectric stepper motor under the beam with a step size around 0.5 μm. By translating the sample in this manner a series of Laue patterns is obtained, and two-dimensional maps of stress, strain and orientation can be produced. Table 1 lists the parameters used to scan the three samples considered in this work, with the corresponding area and number of Laue images collected. All scans were performed at room temperature.

4. Results

Fig. 1 shows typical maps of data that can be obtained from the microdiffraction experiment and subsequent analysis. These gray-scale images show the angle between the $\langle 1\,1\,1\rangle$ direction and the film normal. Grain outlines have been overlaid to mark the boundaries between grains. Our ability to determine the exact location of the grain boundary is limited by the step size of the microdiffraction scan. Each Laue image can contain diffraction data from several different grains. The principal grain within each volume is determined from the intensities of the Laue spots. However, the misorientation between grains is known very accurately (0.01°), and it is only the position of the grain boundary relative to the two grains that is not known precisely. Therefore the map gives only an approximation of the microstructure, and care should be taken when inferring information about the exact location of grain boundaries. However, for the interest of this work, the statistics provided

Table 1
Microdiffraction experimental parameters; X and Y are the number of diffraction images taken in the x- and y-directions, S is the step size, L_X and L_Y are the total scan lengths, A is the total area, and N is the total number of Laue diffraction images collected

Sample	X	Y	S (μm)	L_X (μm)	L_Y (μm)	A (μm^2)	N
Al(Cu) on Si	97	71	0.4	38.8	28.4	1102	6887
Cu on Al_2O_3 (scan 1)	30	30	0.5	15	15	225	900
Cu on Al_2O_3 (scan 2)	41	41	0.25	10.25	10.25	105	1681

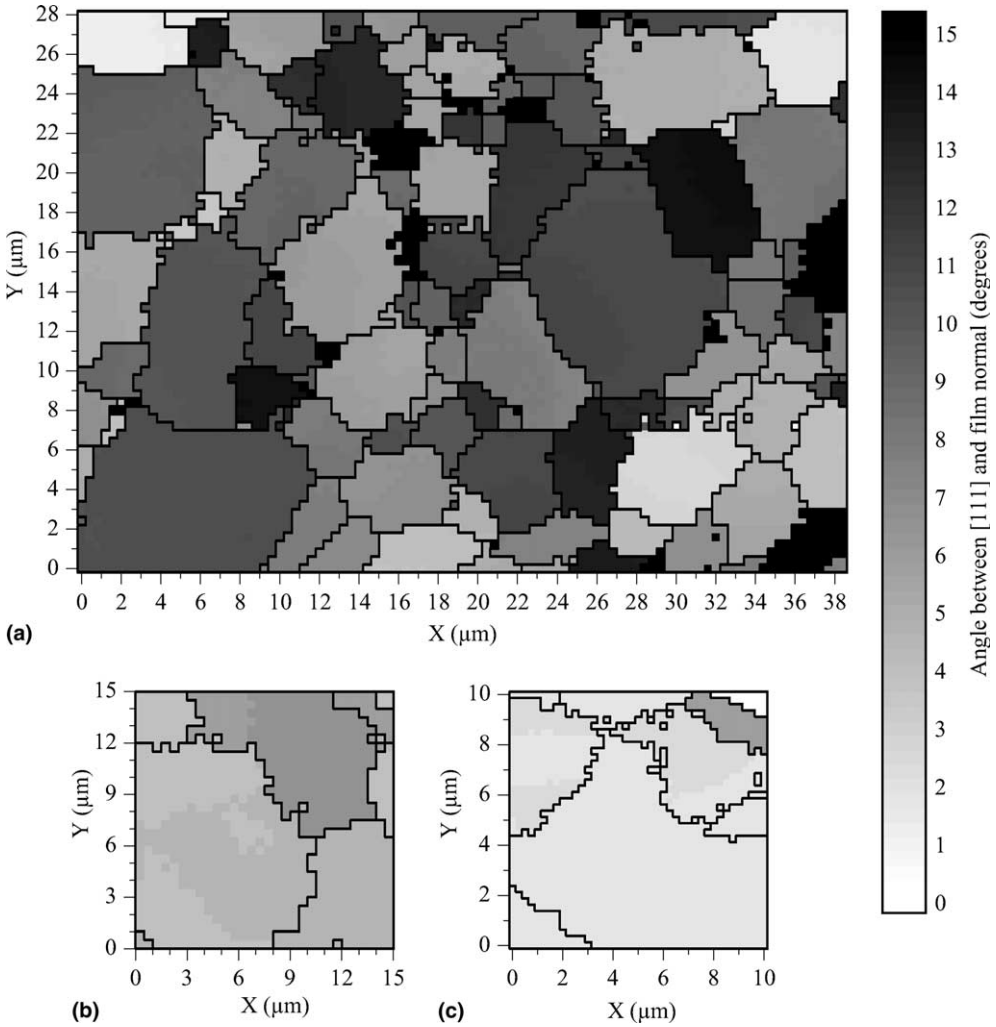

Fig. 1. XRMD map of orientation of the [1 1 1] direction with respect to the film normal for (a) 1.5 μm Al (0.5 wt% Cu) on silicon, and (b) scan 1 and (c) scan 2 of 0.8 μm Cu on Al_2O_3.

by the large number of data points outweighs any uncertainty about the precise positions of grain boundaries.

The Al(Cu) film has a broad (1 1 1) fiber texture, but with only a small number of grains deviating by more than 15° from the film normal. Fig. 2 reproduces the orientation maps for Cu on Al_2O_3 with a new scale so that the misorientation between grains can be more clearly observed. Although these two maps of copper show only a few grains, the images concur with other knowledge about this Cu/Al_2O_3 film [6], and a narrower texture is observed. The larger average grain size and smaller XRMD scan size have resulted in a smaller number of grains that have been sampled.

Fig. 3 shows maps of the maximum resolved shear stress (MRSS) and average peak width (APW) for the Al(Cu) film. Again the outline of grain boundaries is overlaid. The APW is determined from the full width at half maximum of a 2-D Lorenzian fit to the intensity of each spot from a grain in the Laue pattern, and averaging the values obtained. Higher dislocation densities add width to X-ray diffraction peaks. Therefore, the APWs

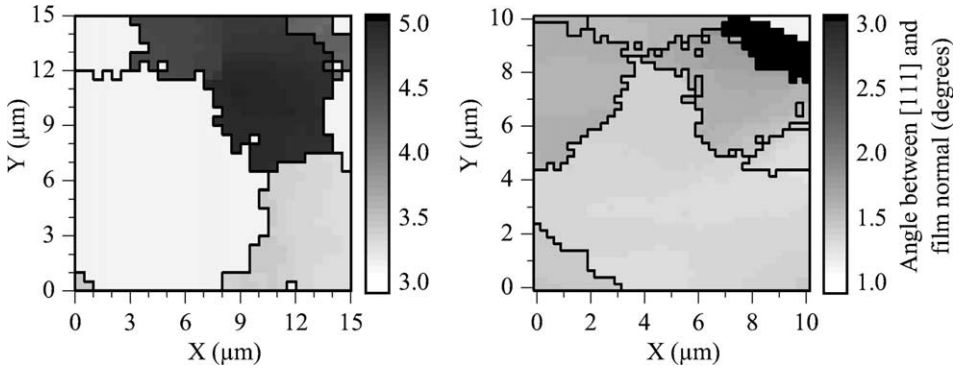

Fig. 2. XRMD maps of orientation of the [1 1 1] direction with respect to the film normal for 0.8 μm Cu on Al_2O_3.

are used here as an indication of relative dislocation density within the grains. Each data point in Fig. 3 is an average of the surrounding 3×3 images (data from neighboring grains are excluded from this averaging step) to smooth the data. Several grains have been labelled (A–E) for discussion below.

In Fig. 4, the median value of the MRSS for Al(Cu) in each grain has been calculated. Grain size is calculated as the square root of the area occupied by the grain in the grain map. This provides a straightforward method of comparing differences between stresses in grains of different size. Fig. 4 also shows a median value calculated by combining all of the MRSS values within the size intervals that are shown on the chart.

Fig. 5 shows maps of the MRSS for the copper film on sapphire. Again, an averaging of the surrounding 3×3 images (data from neighboring grains excluded) was performed. There are an insufficient number of grains in these maps to produce the median chart similar to Fig. 4. Instead, Fig. 6 shows the MRSS data from the two samples after binning into histograms. The MRSS data from the two scans of copper on sapphire have been combined to give one aggregate chart. The two room-temperature scans are comparable, and the data have been combined to give improved statistics. The bottom axis for these histograms has been normalized by dividing the MRSS by the slip plane shear modulus of the thin film material, which is calculated using

$$\mu_{\langle 1\,1\,0\rangle\{1\,1\,1\}} = C_{44} - \frac{2C_{44} + C_{12} - C_{11}}{3}.$$

The following values for the elastic constants have been used: $C_{11} = 106.8$ GPa, $C_{12} = 60.7$ GPa, $C_{44} = 28.2$ GPa (Al); $C_{11} = 168.4$ GPa, $C_{12} = 121.4$ GPa, $C_{44} = 75.4$ GPa (Cu). This gives a slip plane shear modulus of 24.8 GPa for Al, and 40.8 GPa for Cu. The total counts for the Al(Cu) film are higher, but there are still good statistics for comparison of both data sets.

5. Discussion

In both samples considered here, the final stress state is obtained after temperature cycling, so that the total strain imposed is produced by mismatch between thermal expansion of the film and substrate, and is given by

$$\varepsilon_{\text{total}} = \Delta\alpha\Delta T,$$

where $\Delta\alpha$ is the difference between the coefficients of thermal expansion of the film and substrate, and ΔT is the change in temperature. This equi-biaxial total strain induced by the substrate produces a plane-stress state on average. Therefore, the same total strain has been applied locally. The level of stress that would be measured if all of this strain was accommodated by elastic deformation is

$$\sigma_{\text{total}} = M\Delta\alpha\Delta T,$$

where M is the biaxial modulus of the film. The anisotropic biaxial modulus in the (1 1 1) plane of

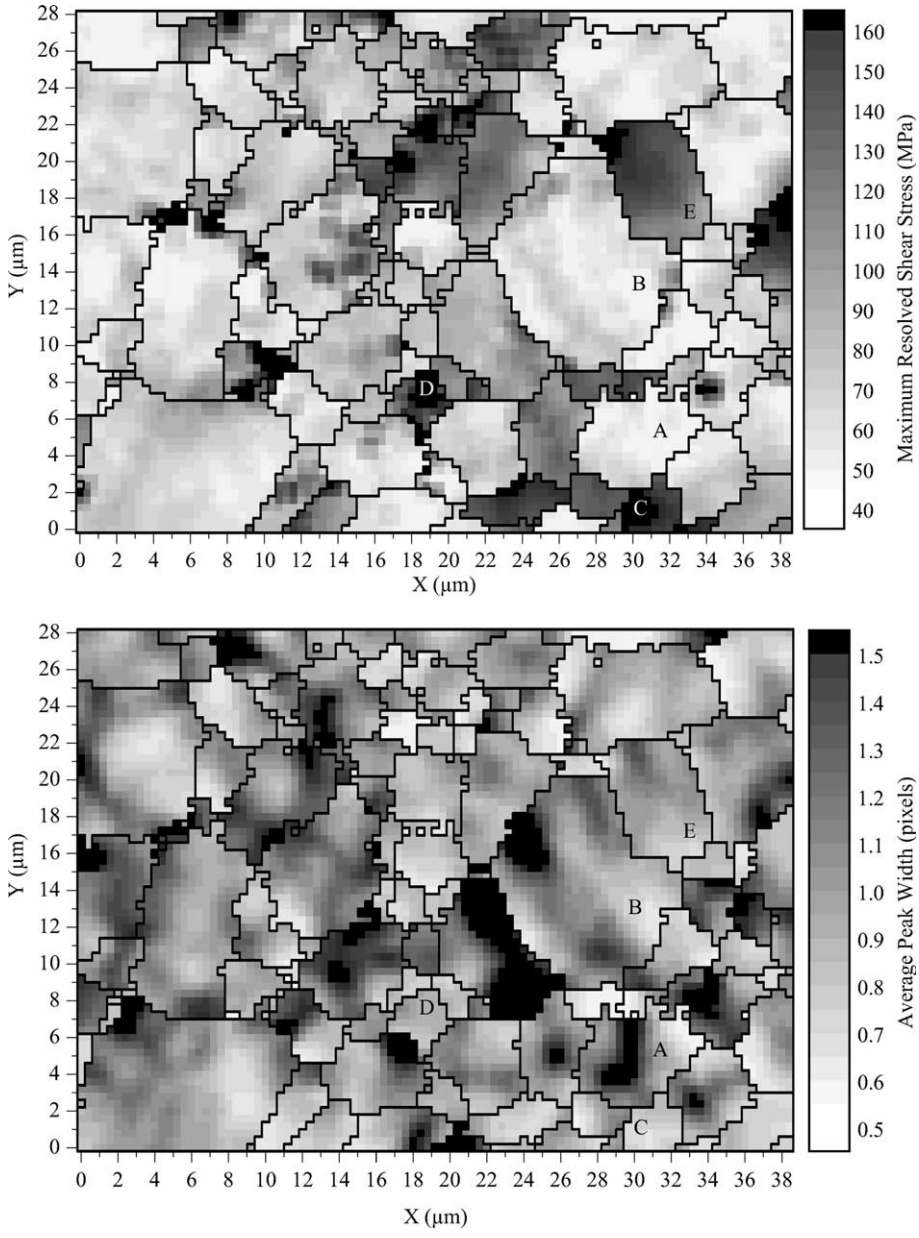

Fig. 3. XRMD maps of maximum resolved shear stress (MRSS) and average peak width (APW) for 1.5 μm Al (0.5 wt% Cu) on silicon. The pixel unit refers to pixels on the CCD camera and roughly corresponds to $\Delta 2\theta = 0.1°$.

Al is 110 GPa, and of Cu is 260 GPa. The change in temperature from 400 °C to room temperature is $\Delta T = 375$ K. The coefficients of thermal expansion are taken as; $\alpha_{Al} = 23 \times 10^{-6}$ K^{-1} [6], $\alpha_{Si} = 2.5 \times 10^{-6}$ K^{-1} [14], $\alpha_{Cu} = 18 \times 10^{-6}$ K^{-1} [6], $\alpha_{Al_2O_3} = 7 \times 10^{-6}$ K^{-1} [6]. Therefore, the expected total biaxial stress is around 850 MPa for Al(Cu) on Si, and 1070 MPa for Cu on Al_2O_3. This would then correspond to a resolved shear stress of 265 MPa for Al(Cu)/Si and 340 MPa for Cu/Al_2O_3 on one of the $\langle 1\,1\,0\rangle\{1\,1\,1\}$ slip systems. However, the values of MRSS in Figs. 3–5 are lower than these

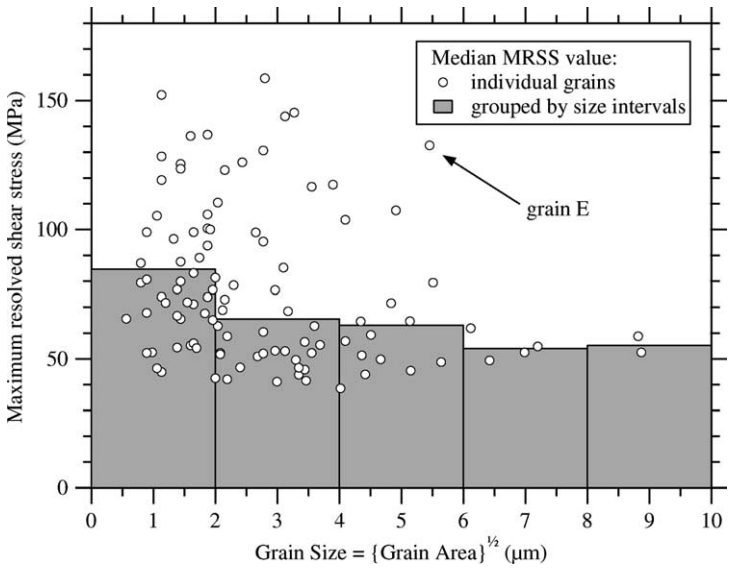

Fig. 4. Median MRSS versus grain size for 1.5 μm Al (0.5 wt% Cu) on silicon (calculated for each grain in Fig. 3). The histogram shows the median values when the data has been grouped into the size intervals shown. Grain E is labelled in Fig. 3 and discussed in the text.

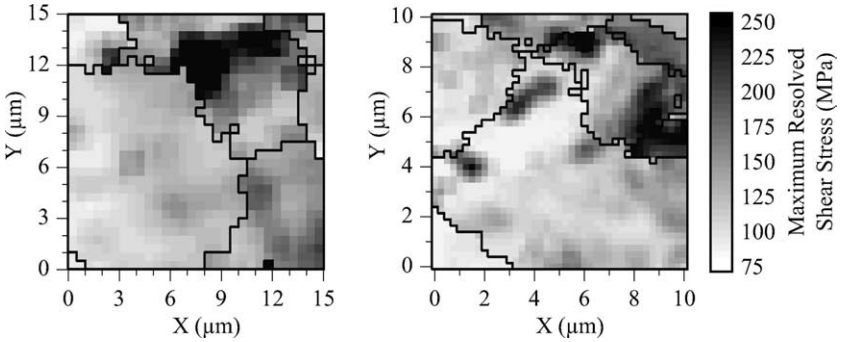

Fig. 5. XRMD maps of MRSS for 0.8 μm Cu on Al_2O_3.

predicted maxima supporting the conclusion that substantial plastic deformation has occurred throughout the film.

First consider the case of the polycrystalline Al(Cu) film. The map of maximum resolved shear stress in Fig. 3 shows that the differences in yielding behavior range from many grains with a MRSS of 40–60 MPa to several grains (and regions within grains) that have values of MRSS greater than 160 MPa. This can also be observed in Fig. 4, where in general the larger grains have lower median MRSS values. In comparison, the smaller grains have a range of values; on average the smaller grains have a higher median MRSS, but when considered individually, some have the same low median level of MRSS as the large grains. The large MRSS in some small grains suggests that substantially less plastic deformation has occurred there. This result is also confirmed by the map of average peak width, where a grain with a low MRSS corresponds with a region of high APW (e.g. grains labelled A and B), or regions of high MRSS have a low APW (e.g. grains labelled C and D).

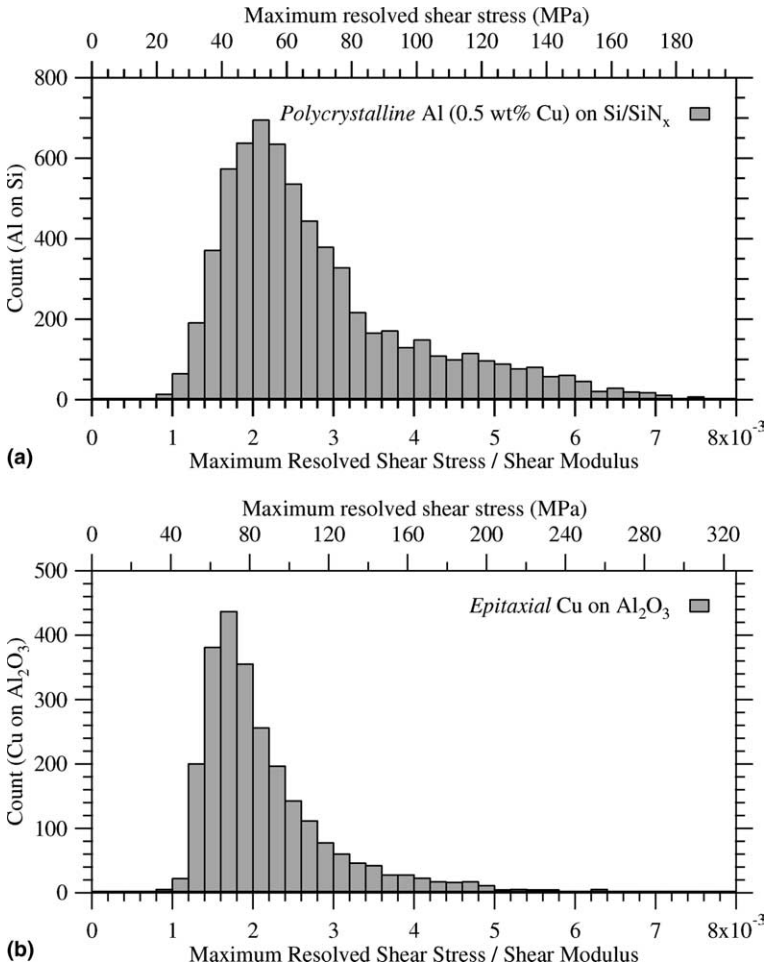

Fig. 6. Histograms of MRSS values from polycrystalline Al(Cu) on Si, and epitaxial Cu on Al_2O_3 (data from scans 1 and 2 have been combined to improve statistics). Shear stress has been normalized by dividing by the slip plane shear modulus.

Fig. 4 reveals what appears to be a lower bound to the MRSS data at around 40–45 MPa. This could be a situation where a sufficient number of dislocation sources are available so that once yielding has occurred the final level of the stress state is determined by the Nix–Freund model given in Eq. (1). As the grain size in these films is generally much larger than the film thickness, this form of the Nix–Freund model can be applied. Unfortunately, it is difficult to predict what this low MRSS value is for the Al(Cu) because the film is not pure aluminum. For pure Al on Si with $h = 1.5$ μm; $\mu_f = 26$ GPa, $\mu_s = 66.5$ GPa, $b = 2.86$ Å, $\nu = 0.34$–0.5, $\beta = 2.6$, $\sin\phi/(\cos\phi\cos\lambda) = 3.46$, this model predicts a biaxial stress of 29–37 MPa, or a resolved shear stress of 9–12 MPa. This is lower than the observed lower bound to the data, even when the experimental error (17 MPa for Al) is considered. However, this model does not take into account any additional hardening that has occurred in the Al(Cu) film. There are at least two additional factors; alloying additions and strain hardening. The Nix–Freund model predicts the critical stress for the first yielding event, and does not account for any strain hardening. Several dislocation dynamics models [15,16] have shown that the stresses required to lay down additional dislocations are higher than the stresses predicted

by the Nix–Freund model. Several authors have suggested precipitation hardening as an additional mechanism that increases the low-temperature strength of Al(Cu) films over that of pure Al films during thermal cycling [1,17,18].

The comparison between the polycrystalline Al(Cu) and the epitaxial Cu films is instructive. We find very similar peak values of the MRSS when normalized by the shear stress. However, there is a much broader distribution of MRSS in the Al film than in the Cu film. Several reasons for this are possible. (a) Epitaxial films have a large average grain size. As seen in the Al(Cu) film, large grains tend to have lower values of MRSS. Therefore, large grains in the epitaxial film might be considered representative of the entire film, whereas in the polycrystalline film the grain size distribution is much broader, containing many smaller grains with higher stresses, which produces the broader distribution of stresses. (b) An alternate explanation may lie in an insufficient number of dislocation sources in polycrystalline films. This speculation is supported by the work of Dehm et al. [6] who show that in epitaxial films, misfit dislocations at the film/substrate interface can act as sources for dislocations. Intuitively, one might assume that polycrystalline films have a large number of nucleation sites, but Dehm et al. [6] also reported that dislocations were not emitted from the interface between the metal film and amorphous interlayer in these films. Thus, in polycrystalline films, the only sources for dislocations are grain boundaries and triple junctions. Owusu-Boahen and King [9] suggest that yielding can occur only at special triple junctions, thereby further limiting the number of dislocation sources in polycrystalline films. The exact configuration of the grain boundaries is not known for these samples, so the Owusu-Boahen/King hypothesis cannot be directly applied. However, limited nucleation sites and absence of interfacial sources would provide an explanation as to why there are such large variations in stress from grain to grain in the polycrystalline film. More work is required to substantiate this claim.

It is also clear from the maps in Figs. 3 and 5 that in both the polycrystalline and the epitaxial films, large local differences in yielding have occurred. MRSS is used as the measure of plasticity; regions with low MRSS values (lighter) have yielded more than regions with high MRSS values (darker). There are large differences between grains, but also substantial variations within grains.

As discussed previously [11], the grains in the Al(Cu) film deform inhomogeneously. If an existing set of dislocations is sufficiently aligned, they can form low angle-boundaries, so that further dislocation activity is confined to sub-grains. i.e. the effective grain size is reduced. This can be seen in the grain labelled 'A' in Fig. 3 where a band of increased APW values is apparent. Fig. 7 shows a magnified map of the out-of-plane orientation. The gradient scale has been altered so that the change in orientation across the grain becomes apparent.

Finally, while small grains tend to display less plasticity, this is not always the case. Some unusual grain behavior occurs, such as the grain labelled E (also marked in Fig. 4) which has a relatively large grain size, a high MRSS and an intermediate range of values for the APW. However, a closer examination of the MRSS map in Fig. 3 shows that grain E is surrounded entirely by grains with low values of MRSS. It may be that the high MRSS in grain E is correlated with the stress state of the neighboring grains, and local interaction between neighboring grains has an important influence on the yielding behavior.

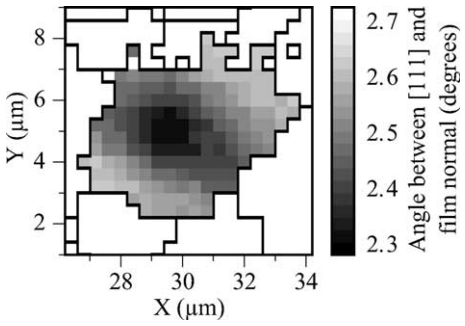

Fig. 7. XRMD map of orientation of the [1 1 1] direction with respect to the film normal for 1.5 μm Al (0.5 wt% Cu) on silicon. This map is of the grain labelled 'A' in Fig. 3.

6. Conclusions and summary

When investigated by microdiffraction, the stress states in thin metal films appear much more complex than as assumed in simple models. It is determined by the interaction of the applied thermal strain with the grain microstructure and dislocations. Some of the observations made in this report are;

- Large local differences in stress have been observed in a polycrystalline Al (0.5 wt% Cu) film on Si and epitaxial Cu film on Al_2O_3. Differences are apparent between grains, but also within grains.
- While both types of film display a variation in plasticity, the width of the distribution is much broader in the polycrystalline film.
- In the polycrystalline Al(0.5 wt% Cu) film on Si, large grains often have lower MRSS values, and small grains can have a range of stresses.
- Local interaction between neighboring grains may also be an important mechanism for polycrystalline films, where there are a limited number of dislocation sources. This is thought to be partly responsible for the nonuniform stresses within the film.

From an application point-of-view, localization of yielding is undesirable, as sites of high residual stress are principal locations for formation of voids or other deleterious microstructural defects. In microelectronic and micromechanical systems, such defects can lead to early failure in service. Further understanding of how these stress maxima occur can lead to their prevention. In terms of processing, very sharp textures, uniform grain size and the absence of special triple junctions are highly desirable.

Acknowledgements

The Advanced Light Source is supported by the Director, Office of Science, Office of Basic Energy Sciences, Materials Sciences Division, of the US Department of Energy under contract No. DE-AC03-76SF00098 at Lawrence Berkeley National Laboratory. The authors would like to thank H. Edongué and G. Dehm from the Max-Planck-Institut für Metallforschung for providing the epitaxial copper on sapphire sample.

References

[1] R. Venkatraman, J.C. Bravman, W.D. Nix, P.W. Davies, P.A. Flinn, D.B. Fraser, Journal of Electronic Materials 19 (11) (1990) 1231–1237.
[2] D. Weiss, H. Gao, E. Arzt, Acta Materialia 49 (13) (2001) 2395–2403.
[3] W.D. Nix, Metallurgical Transactions A 20 (11) (1989) 2217–2245.
[4] J.E. Sanchez Jr., E. Arzt, Scripta Metallurgica et Materialia 27 (3) (1992) 285–290.
[5] L.B. Freund, Advances in Applied Mechanics 30 (1994) 1–66.
[6] G. Dehm, T.J. Balk, H. Edongué, E. Arzt, Small-scale plasticity in thin Cu and Al films, Microelectron. Eng. 70 (2003) 412–424.
[7] C.V. Thompson, Journal of Materials Research 8 (2) (1993) 237–238.
[8] B.J. Inkson, G. Dehm, T. Wagner, Acta Materialia 50 (20) (2002) 5033–5047.
[9] K. Owusu-Boahen, A.H. King, Acta Materialia 49 (2) (2001) 237–247.
[10] S. Krämer, J. Mayer, C. Witt, A. Weickenmeier, M. Rühle, Ultramicroscopy 81 (3–4) (2000) 245–262.
[11] R. Spolenak, W.L. Brown, N. Tamura, A.A. MacDowell, R.S. Celestre, H.A. Padmore, B. Valek, J.C. Bravman, T. Marieb, H. Fujimoto, B.W. Batterman, J.R. Patel, Physical Review Letters 90 (9) (2003) 096102/1–096102/4.
[12] A.A. MacDowell, R.S. Celestre, N. Tamura, R. Spolenak, B. Valek, W.L. Brown, J.C. Bravman, H.A. Padmore, B.W. Batterman, J.R. Patel, Nuclear Instruments and Methods in Physics Research A 467 (2001) 936–943.
[13] N. Tamura, R.S. Celestre, A.A. MacDowell, H.A. Padmore, R. Spolenak, B.C. Valek, N.M. Chang, A. Manceau, J.R. Patel, Review of Scientific Instruments 73 (3) (2002) 1369–1372.
[14] D.E. Gray (Ed.), American Institute of Physics Handbook, third ed., McGraw-Hill, New York, 1972, pp. 4–129.
[15] P. Pant, K.W. Schwarz, S.P. Baker, Acta Materialia 51 (11) (2003) 3243–3258.
[16] B. von Blanckenhagen, P. Gumbsch, E. Arzt, Philosophical Magazine Letters 83 (1) (2003) 1–8.
[17] A. Witvrouw, J. Proost, P. Roussel, P. Cosemans, K. Maex, Journal of Materials Research 14 (4) (1999) 1246–1254.
[18] D. Jawarani, H. Kawasaki, I.S. Yeo, L. Rabenberg, J.P. Stark, P.S. Ho, Journal of Applied Physics 82 (1) (1997) 171–181.